

Step Work: Wind Tunnel Investigation of Stepped NACA 0012 Airfoils in the Low Reynolds Number Regime

Alahe Akhavan, Nola Brady, Angel Hernandez, James Hoadley

University of California, Berkeley
Fall 2025

Abstract

At low airspeeds, any small geometric changes to an airfoil can have huge impacts on airfoil performance. This is due to viscous effects that influence separation of the flow, inducing drag and stall. This report aims to compare a standard NACA 0012 airfoil against two modified Kline-Fogleman stepped airfoils. The two cases are one step at 50 percent of the airfoil or two steps, one at 25 percent and another at 50 percent chord length. Wind tunnel tests at varying angles of attack ($\alpha = 0^\circ, 4^\circ, 10^\circ, 12^\circ, 14^\circ$, and 16°) and airspeeds allowed for strain-gage measurements for lift. Stall onset appeared to start near ($\alpha \approx 10^\circ$) to (12°) in all test cases for all airfoils. The stepped airfoils approached thin-airfoil predictions over the assumed alpha range below the stall angle. Hypothesis testing indicates the 1-step (S1) configuration produced statistically significant lift differences relative to the baseline. These results motivate further testing over a wider set of conditions and step geometries.

1 Introduction

1.1 Motivation and Background

Since airfoil geometry already is known to play the most important role in aerodynamic performance. This sensitive difference is seen the most at low airspeeds. This is because at low Reynolds numbers, viscous effects strongly influence the physical properties of the airfoil, most notably lift, drag, and stall angle. Boundary layer separation is strongly affected in this regime by small geometric differences between airfoils. One such historical modification is the Kline-Fogleman stepped airfoil family. In this paper, we introduce modified Kline-Fogleman airfoils S1 and S2 for one-stepped and two-stepped airfoils based on the NACA 0012 airfoil. This is at 25 percent and 50 percent chord length. Having steps in an airfoil would trip the airflow over an airfoil by creating trapped vortices that reduce airfoil separation, while also reducing skin friction drag, which aims to delay stall. Does introducing steps to an airfoil change the aerodynamic performance compared to a baseline NACA 0012 airfoil under standard atmospheric conditions?

1.2 Related Work

Previous studies have shown that airfoil aerodynamic behavior is highly sensitive to Reynolds number, particularly in low-Reynolds-number regimes where viscous effects influence lift generation, drag characteristics, and stall behavior [1][2]. For symmetric airfoils such as the NACA 0012, classical theory predicts a linear lift response only within a limited pre-stall angle-of-attack range, with deviations and earlier stall onset occurring as Reynolds number decreases [1].

Tirandaz and Rezaeiha demonstrated that symmetric airfoil shape significantly influences power performance and stall behavior in dynamically stalled vertical-axis wind turbine applications, showing the sensitivity of low-Re flows to geometric features and unsteady separation effects [2]. While the research study suggest potential performance benefits from geometric modification, reported results depend strongly on operating conditions, Reynolds number, and specific geometric parameters. One takeaways is that the surface discontinuities can alter boundary-layer behavior, pressure distribution, and separation characteristics.

1.3 Objectives and Scope

This experiment compares the NACA 0012 airfoil to two modified Kline-Fogleman variants, one at 25 percent and one at 50 percent and 25 percent chord length. Tests aim to measure across multiple airspeeds and angles to capture both pre-stall and post-stall behavior. This ideally would show convergence in pre-stall angles to thin airfoil theory. The scope is limited to these discrete operating points and the specific step placements tested because it envelops the expected stall angle at all available Reynolds numbers.

1.4 Design of Custom Stepped Airfoils

Kline-Fogleman modified airfoils, sometime called stepped airfoils, in practice are typically custom airfoils that full a rule for the number of steps and it's location. The design of two-step airfoils is derived from the surface outline of a standard NACA 0012 airfoil, and then modified with a step at a specified percent chord length. The two custom are named S1 KFm-NACA 0012 ($N_s = 1$) and S2 KFm-NACA 0012 ($N_s = 2$), for one and two steps respectively. The reasons for the NACA 0012 part is to denote it is a NACA 0012 derivative; however it can be dropped for brevity. These two custom airfoils, in additional to a standard NACA 0012, is our design space for the experiment. The following table describes where the steps for each airfoil are located. Additionally, the the thickness for the steps closet to the

Airfoil	Chord c (in)	Span b (in)	Step One (in)	Step Two (in)
NACA 0012	5	9.78	N/A	N/A
S1 KFm	5	9.78	0.5c	N/A
S2 KFm	5	9.78	0.25c	0.5c

Table 1: Major Airfoil Dimensions

trailing edge is $t_{TE} = 0.02c$. The thickness of the step near the quarter chord, for S2 KFm, is $t_{c/4} = 0.03c$ from a line tangent to the quarter chord.

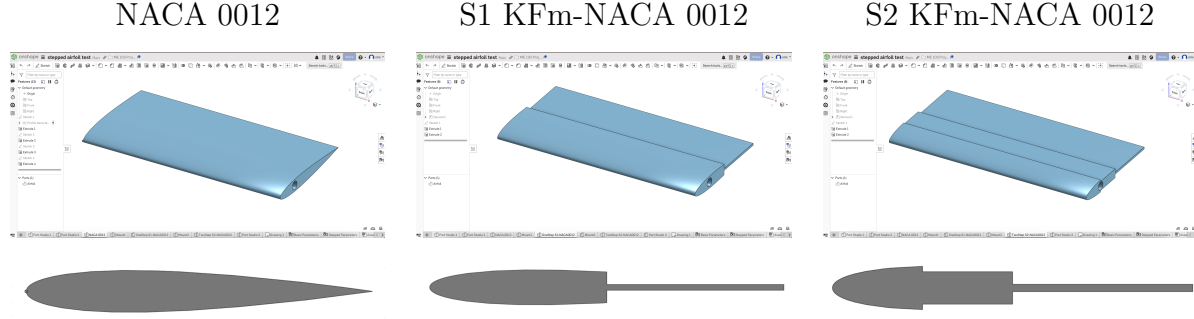


Figure 1: CAD Designs and Surface Profiles

1.4.1 Protractor Mount Design

The mount was designed for the digital protractor placement on the airfoils to set angles of attack. Its only purpose is to help set the angle of attack accurately and then be placed out of the test section. It is dimensioned precisely to be a tight fit tolerance, approximately within the 0.02 tolerance on each side of the airfoils. The outer dimensions are 0.95 x 5.33 in.

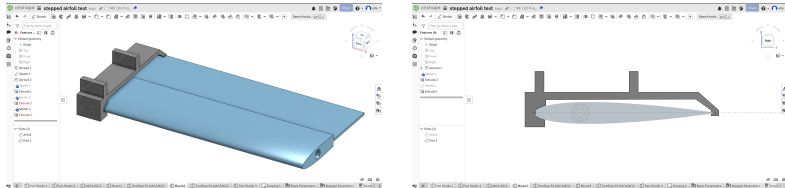


Figure 2: Protractor Mount

2 Method

2.1 Experimental Setup

The experimental process followed a consistent sequence for all 3 airfoil models. Each airfoil was secured in the test section component of the wind tunnel and leveled. We used a digital protractor to set the angle of attack, using a CAD modeled mount part, placed on top of each airfoil. Figure 3 shows visually how the airfoil was mounted and how the protractor set the angle of attack. To measure drag, the airfoil was rotated 90 degrees, using the testing section chord to turn it such that it was perpendicular to the flow. We set the wind tunnel controller to the desired freestream velocity, and tested several tunnel speeds for each configuration. Tests were conducted at:

$$\alpha = 0^\circ, 4^\circ, 10^\circ, 12^\circ, 14^\circ, 16^\circ.$$

Recorded data during each run included: Strain-gage voltage (V), and Pitot-tube pressure (mmHg). The significance of Strain-gage voltage and Pitot-tube pressure raw signals form the basis for calculating lift L and Drag D , and non-dimensional aerodynamic coefficients.

Mounting Airfoil and Setting α Wind Tunnel Test Data Collection

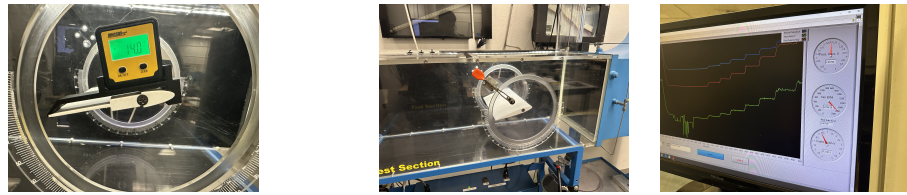


Figure 3: Experimental Procedure

2.2 Calibration

The calibration parameters were selected based on their direct relationship to the controllable inputs and measured outputs of the wind tunnel system. Motor speed and Pitot-tube pressure were chosen to calibrate freestream airspeed because they respectively set and directly sense the flow conditions within the test section. Strain gauge voltage was calibrated using known weights to establish a reliable mapping between the force balance output and the aerodynamic forces acting on the airfoil.

1. Relative Airspeed: we used motor speed as a calibration parameter because it controls the fan operation and therefore sets the flow conditions in the wind tunnel. By correlating motor speed with measured airspeed, we established a reliable relationship that allows repeatable tunnel settings for all of the experiments.
2. Relative Airspeed: Pitot tube pressure was used for calibration because it directly measures the dynamic pressure of the flow, which is physically related to airspeed through Bernoulli's principle. Calibrating airspeed against Pitot pressure ensures that velocity measurements are grounded in the actual flow conditions within the test section.
3. Calibration Weight Table: we used average strain gauge as a calibration parameter because the force balance converts applied aerodynamic loads directly into electrical signals. By calibrating voltage against known applied weights, we established a direct mapping between measured voltage and physical force.

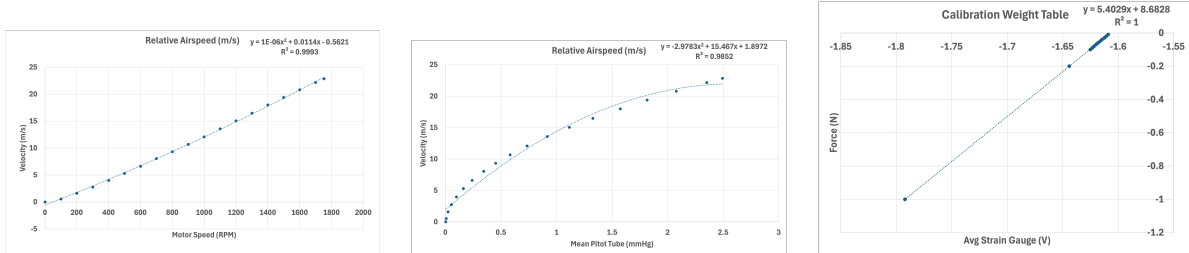


Figure 4: Calibration Plots

Measured Parameter	Symbol	Uncertainty (\pm)
Strain Gauge Voltage	V	δV (V)
Pitot Tube Pressure	p	δp (mmHg)

Table 2: Overall Calibration and Measurement Uncertainties for Raw Sensor Data.

2.3 Data Processing and Analysis

Given the raw data from the pitot tube (mmHg) tube and strain gauge (V), the average for each trace is found. This is then stored at a single data point at a given angle of attack and speed. The conversion from pressure to velocity from Bernoulli's Principle [3]

$$U_\infty = \sqrt{\frac{2p}{\rho_{\text{air}}}} \quad (1)$$

Note that the conversion from mmHg to Pa is at room temperature 20° C [3] is

$$p = 132.3p^{\text{mmHg}} \text{ [Pa]} \quad (2)$$

At room temperature the density of air is $\rho_{\text{air}} = 1.21 \left[\frac{\text{kg}}{\text{m}^3} \right]$. To convert from a voltage to a weight (force) is given by the calibration curve. The function is

$$F = 5.4029V + 8.6828 \text{ [N]} \quad (3)$$

To calculate the lift and drag forces for each angle of attack, the difference between the measured force at zero airspeed and the current airspeed is used. description is

$$L = |F_y(U_\infty) - F_{y,0}| \quad (4)$$

$$D = |F_x(U_\infty) - F_{x,0}| \quad (5)$$

Then, to calculate the coefficient of lift and drag, respectively for the airfoil [3]

$$C_L = \frac{L}{q_\infty S} \quad C_D = \frac{D}{q_\infty S}$$

The sectional coefficients are defined per unit span. Their mathematical definition is [3]

$$c_\ell = \frac{L'}{q_\infty c} \quad (6)$$

$$c_d = \frac{D'}{q_\infty c} \quad (7)$$

Note the lowercase subscript for each and L' and D' , which are the lift per unit span and drag per unit, respectively, i.e., $L = \int_S L' dy$ and $D = \int_S D' dy$. Wing tip effects become negligible when the airfoil becomes infinite, i.e., it spans nearly the entire testing space. This will approximate thin-airfoil theory conditions, while also measuring drag. Within this experiment, it is assumed that the lifting distribution will be approximately elliptical, i.e.

$$c_\ell \approx C_L \quad c_d \approx C_D$$

where $C_D = C_{D_0} + C_{D_i}$. The zero lift drag coefficient, C_{D_0} , is drag due to viscous effects (skin drag) and pressure (form) drag. The induced drag coefficient, C_{D_i} , is the induced drag due to lift. This experiment does not attempt to directly measure the zero-lift drag, but it can be approximated as $C_{D_0} = C_D - C_{D_i}$, where C_{D_i} can be calculated using equations from lifting-line theory. Given that the experimental set-up will limit the effects of the wing-tip vortices (2D airfoil), the total sectional drag coefficient will be of the form [4]

$$c_d = c_{d,\min} + k(c_\ell - c_{\ell,\min})^2$$

where k is an empirical constant obtained from curve fitting with the linear lift region. $c_{d,\min}$ and $c_{\ell,\min}$ are the minimum measured c_d and c_ℓ values respectively. [4] The table below provides a summary of the mathematical relationships used for a symmetrical airfoil Note

Plot	Mathematical Relationship
c_ℓ v α	$c_\ell = m\alpha$
c_d v α	$c_d = c_{d,\min} + k(c_\ell - c_{\ell,\min})^2$
$\frac{c_\ell}{c_d}$ v α	$\frac{L}{D} = \frac{C_L}{C_D} \approx \frac{c_\ell}{c_d}$

Table 3: Aerodynamic Coefficients

that wing-tip effects cannot necessarily be ignored, but, to simplify analysis, they are not directly calculated under the assumption $c_d \approx C_D$. Another simplification is that, since all airfoils are symmetric, $c_{\ell,\min}$ occurs at $\alpha = 0^\circ$ and should always have zero lift. [3]

3 Results

3.1 Summary of Measurements

Since there are a total of seven different Reynolds numbers, measurements were taken at each of them; only the three that are typically reported in simulations are literature for resolution. (see Appendix 6.1) $\text{Re} = \{5 \times 10^4, 1 \times 10^5, 2 \times 10^5\} \approx \{6.20 \times 10^4, 1.08 \times 10^5, 2.00 \times 10^4\}$

Table 4: Lift (c_ℓ) and Drag (c_d) Sectional Coefficients for NACA 0012, S1 KFm, and S2 KFm at $\text{Re} \approx 6.20 \times 10^4$. Rounded to 3 Significant Figures.

Angle of Attack (α in deg)	NACA 0012		S1 KFm		S2 KFm	
	c_ℓ	c_d	c_ℓ	c_d	c_ℓ	c_d
0	-0.0211	0.0337	-0.0377	0.0342	-0.0496	0.0556
4	0.296	0.0541	0.425	0.0937	0.408	0.0882
10	0.741	0.161	1.08	0.228	1.02	0.328
12	0.910	0.317	1.04	0.375	1.07	0.399
14	0.977	0.371	1.07	0.486	1.08	0.474
16	0.920	0.436	1.08	0.499	1.11	0.442

Table 5: Lift (c_ℓ) and Drag (c_d) Sectional Coefficients for NACA 0012, S1 KFm, and S2 KFm at $\text{Re} \approx 1.08 \times 10^5$. Rounded to 3 Significant Figures.

Angle of Attack (α in deg)	NACA 0012		S1 KFm		S2 KFm	
	c_ℓ	c_d	c_ℓ	c_d	c_ℓ	c_d
0	-0.0442	0.016	-0.0341	0.035	-0.0451	0.0518
4	0.345	0.0454	0.417	0.11	0.407	0.0764
10	0.862	0.189	1.14	0.232	1.08	0.274
12	0.983	0.316	1.18	0.378	1.14	0.395
14	0.978	0.400	1.10	0.449	1.13	0.440
16	0.938	0.450	1.11	0.504	1.13	0.418

Table 6: Lift (c_ℓ) and Drag (c_d) Sectional Coefficients for NACA 0012, S1 KFm, and S2 KFm at $\text{Re} \approx 2.00 \times 10^5$. Rounded to 3 Significant Figures.

Angle of Attack (α in deg)	NACA 0012		S1 KFm		S2 KFm	
	c_ℓ	c_d	c_ℓ	c_d	c_ℓ	c_d
0	-0.0244	0.0124	-0.0333	0.0341	-0.0428	0.0114
4	0.389	0.0525	0.416	0.0889	0.401	0.0612
10	0.973	0.232	1.17	0.227	1.14	0.246
12	1.14	0.234	1.17	0.374	1.08	0.350
14	1.06	0.397	1.23	0.488	1.08	0.350
16	0.977	0.413	1.14	0.496	1.14	0.408

Table 7: Overall Calibration Uncertainties for Aerodynamic Measurements

Measured Parameter	Uncertainty (\pm)
Angle of Attack (α)	$u_\alpha = 0.2$ (deg)
Lift Coefficient (c_ℓ)	δc_ℓ
Drag Coefficient (c_d)	δc_d

3.2 Trends and Plots

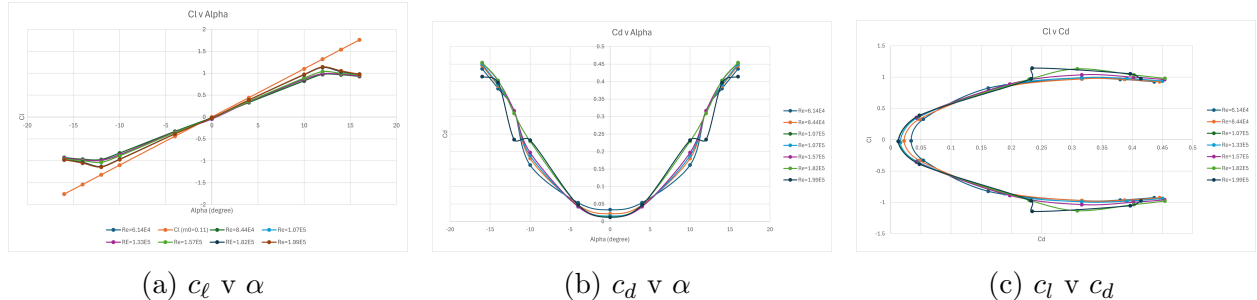


Figure 5: NACA 0012 Aerodynamic Coefficients

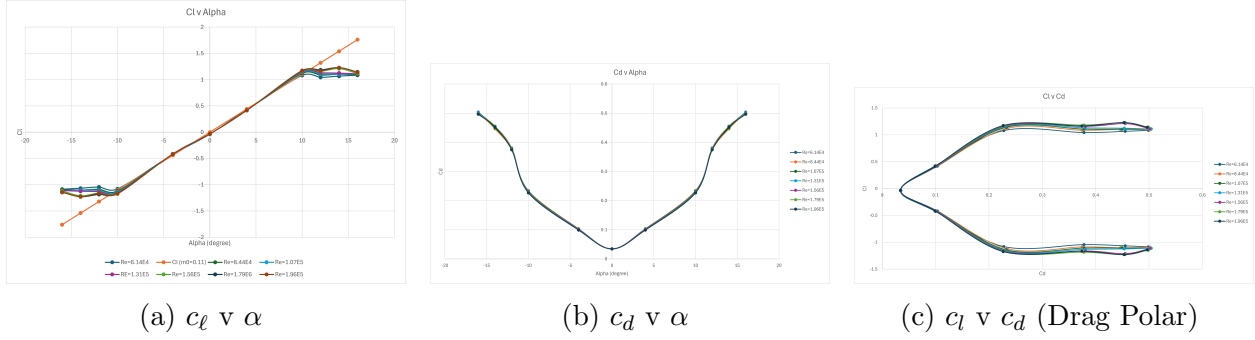


Figure 6: S2 KFm (-NACA 0012) Aerodynamic Coefficients

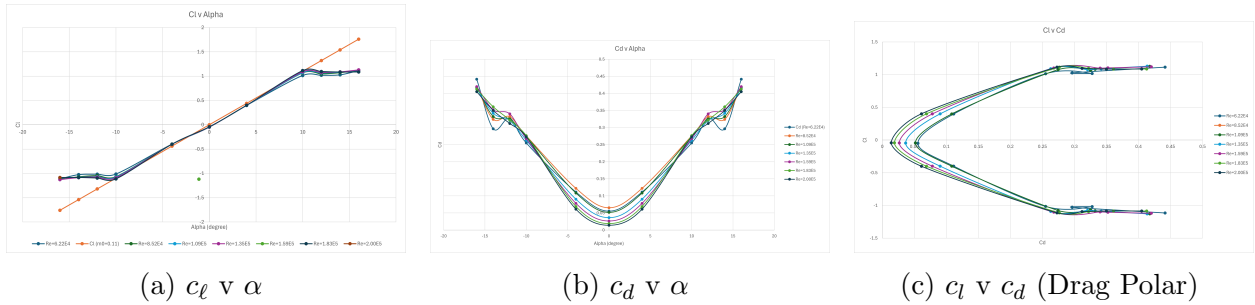


Figure 7: S1 KFm (-NACA 0012) Aerodynamic Coefficients

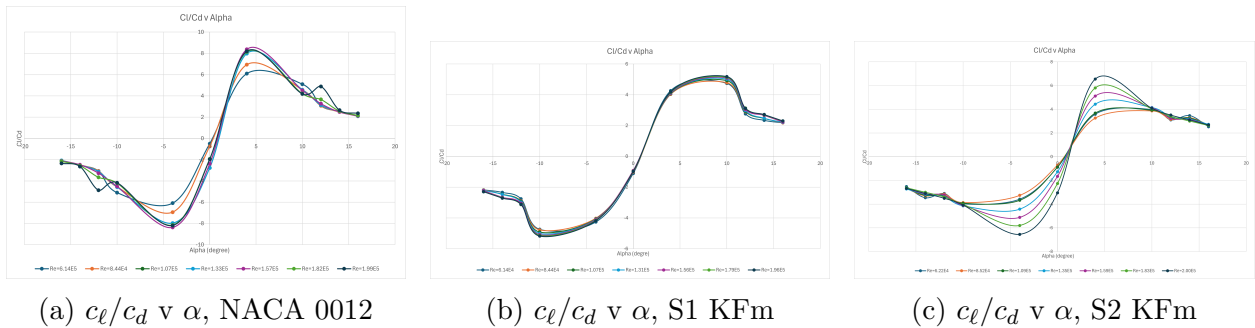


Figure 8: Lift-to-Drag Ratio Comparison

4 Discussion

4.1 Interpretation of Results

The approximate stall angle occurs around $10 - 12^\circ$ degrees for all airfoils. Another major observation is that the slope of the coefficient versus angle of attack curve for both stepped airfoils converges to that of the thin airfoil slope, $m_0 = 2\pi (= 0.11 c_l/\text{deg})$, within 9% of the theoretical sectional lift coefficient (Appendix 6.2). This implies that even at lower Reynolds numbers that are within the overall laminar flow regime, the local flow is turbulent, i.e., at higher Reynolds numbers, which is representative of an inviscid flow. This means that the stepped airfoil is working as claimed, by reducing the effects of skin friction (viscous drag) and form drag (pressure drag), which are dominant in laminar flow regimes.

Another observed behavior is that the stepped airfoils have a post-stall behavior, from the data, which appears to have a slower drop off compared to NACA 0012. This post-stall behavior can not be confirmed since the angle at which the airfoil does not produce any lift is not known, a limitation of the design of the experiment itself, due to constraints.

4.2 Comparison to Literature

All airfoils considered (NACA 0012, S1-KFm, and S2-KFm) have a maximum thickness of 12% of the chord, allowing them to be modeled as thin airfoils. Historical experimental data suggest that actual values are within 10% of the theoretical limit $m_0 = 2\pi$ [3]. In this study, a conservative linear range of $-10^\circ \leq \alpha \leq 10^\circ$ is assumed for all airfoils. Because the experiments were conducted at low Reynolds numbers, the slope is not expected to exactly equal 2π , though it approaches this value as the Reynolds number increases. Accordingly, the lift-curve slope is approximated as

$$m \approx \frac{\Delta c_\ell}{\Delta \alpha}, \quad \alpha \in [-10^\circ, 10^\circ], \quad (8)$$

Comparing to the gathered data, both stepped airfoils converged to m_0 , within the linear range, while the regular NACA 0012 did not for the tested Reynolds' numbers. It did follow an approximately linear curve up until 10° as predicted by simulations and literature.

The drag coefficient c_d is estimated to be of the form

$$c_d = c_{d,\min} + k(c_\ell - c_{\ell,\min})^2 \quad (9)$$

where k is an empirical coefficient from the data. This would be for a purely 2D airfoil, where this assumption is fair, as the airfoil spans nearly the entire cross-section of the wind tunnel.

4.3 Limitations and Uncertainty

The main limitation within this experiment was the time to conduct the experiment. To respect the time of the Hesse Shop Staff, a limited number of angles of attack were tested. From literature, simulations, and prior knowledge, angles of attack from 0° to 10° are approximately linear, even if they do not follow the slope $m_0 = 2\pi$. The explicitly assumptions is that since all airfoils are symmetrical, the data can be reflected about 0° , thus any errors in the positive angles will be directly translated into the negative angles. Since we are interested in pre-stall and post-stall behavior, we focused on measurements for angles above 10° up to 16° .

Uncertainty in the aerodynamic coefficients is caused mainly from angle-of-attack resolution, pitot-tube pressure measurements, and strain-gauge force calibration. Small errors in pitot pressure propagate into freestream velocity and dynamic pressure, while strain-gauge uncertainty directly affects the calculated lift and drag forces. These effects are most seen at lower Reynolds numbers and near stall, where small changes in α lead to large variations in lift. But, since all of our airfoils were tested under the same conditions using the same instrumentation, these uncertainties mostly cancel when comparing configurations.

5 Conclusions

Null hypothesis: under identical atmospheric and wind tunnel conditions, step-modified NACA airfoils do not produce greater lift than the baseline NACA 0012 airfoil at comparable operating conditions. Our findings suggests:

- Statistical comparisons between the one-step modified airfoil and the baseline NACA 0012 showed significant lift differences at Reynolds numbers of $Re = 156,830$ and $Re = 84,383$, with p-values of 0.0385 and 0.0483, respectively.
- Since both p-values fall below the 0.05 significance level, there is sufficient evidence to reject the null hypothesis at these Reynolds numbers.
- These results indicate that step-modified NACA airfoils can achieve increased lift at comparable drag levels relative to the baseline configuration.

5.1 Implications and Future Work

The observed increase in lift at similar drag levels suggests that step-modified airfoils may create performance advantages for small-scale aircraft operating at low Reynolds numbers, where pressure drag effects are low and viscous drag is higher. Future work could investigate the influence of step geometry, including step height and chord-wise placement, as well as extend testing to a broader range of Reynolds numbers.

Acknowledgments

The authors thank the ME 103 course staff at the University of California, Berkeley for their support and guidance throughout the experiment. The authors also acknowledge the Hesse Hall machine shop staff for the time they dedicated to assist with the wind tunnel access and instrumentation setup.

References

- [1] Introduction to Aerospace Flight Vehicles, Embry-Riddle Aeronautical University, eaglepubs.erau.edu/introductiontoaerospaceflightvehicles/chapter/airfoil-characteristics/.
- [2] Tirandaz, M. Rasoul, and Abdolrahim Rezaeiha. "Effect of Airfoil Shape on Power Performance of Vertical Axis Wind Turbines in Dynamic Stall: Symmetric Airfoils." *Ocean Engineering*, vol. 235, 2021, article 105061, doi:[10.1016/j.oceaneng.2021.105061](https://doi.org/10.1016/j.oceaneng.2021.105061).
- [3] Kuethe, Arnold M., and Chuen-Yen Chow. *Foundations of Aerodynamics: Bases of Aerodynamic Design* (5th Ed.). John Wiley & Sons, Inc., 1998.
- [4] Scholz, Dieter (or HAW Hamburg). "13 Drag Prediction." *Aircraft Design Lecture Notes*, HAW Hamburg (Hamburg University of Applied Sciences). Available at: https://www.fzt.haw-hamburg.de/pers/Scholz/H00U/AircraftDesign_13_Drag.pdf.
- [5] Cimbala, John M. "The Turbulent Flat Plate Boundary Layer (Section 10-6, Çengel and Cimbala)." *Course Notes (ME 320)*, Penn State University, Spring 2015. Available at: https://www.me.psu.edu/cimbala/me320web_Spring_2015/pdf/Flat_plate_turbulent_BL.pdf.

6 Appendix

6.1 Summary Data Tables

Table 8: Lift (c_ℓ) and Drag (c_d) Sectional Coefficients for NACA 0012, S1 KFm, and S2 KFm at $\mathbf{Re} \approx 6.20 \times 10^4$. Rounded to 3 Significant Figures.

Angle of Attack (α in deg)	NACA 0012		S1 KFm		S2 KFm	
	c_ℓ	c_d	c_ℓ	c_d	c_ℓ	c_d
0	-0.0211	0.0337	-0.0377	0.0342	-0.0496	0.0556
4	0.296	0.0541	0.425	0.0937	0.408	0.0882
10	0.741	0.161	1.08	0.228	1.02	0.328
12	0.910	0.317	1.04	0.375	1.07	0.399
14	0.977	0.371	1.07	0.486	1.08	0.474
16	0.920	0.436	1.08	0.499	1.11	0.442

Table 9: Lift (c_ℓ) and Drag (c_d) Sectional Coefficients for NACA 0012, S1 KFm, and S2 KFm at $\mathbf{Re} \approx 8.50 \times 10^4$. Rounded to 3 Significant Figures.

Angle of Attack (α in deg)	NACA 0012		S1 KFm		S2 KFm	
	c_ℓ	c_d	c_ℓ	c_d	c_ℓ	c_d
0	-0.0166	0.0223	-0.0354	0.0349	-0.0461	0.0653
4	0.328	0.0475	0.418	0.104	0.417	0.0992
10	0.823	0.18	1.12	0.234	1.1	0.234
12	0.977	0.316	1.18	0.375	1.14	0.376
14	0.963	0.388	1.11	0.446	1.12	0.477
16	0.926	0.445	1.09	0.502	1.12	0.418

Table 10: Lift (c_ℓ) and Drag (c_d) Sectional Coefficients for NACA 0012, S1 KFm, and S2 KFm at $\mathbf{Re} \approx 1.08 \times 10^5$. Rounded to 3 Significant Figures.

Angle of Attack (α in deg)	NACA 0012		S1 KFm		S2 KFm	
	c_ℓ	c_d	c_ℓ	c_d	c_ℓ	c_d
0	-0.0442	0.016	-0.0341	0.035	-0.0451	0.0518
4	0.345	0.0454	0.417	0.11	0.407	0.0764
10	0.862	0.189	1.14	0.232	1.08	0.274
12	0.983	0.316	1.18	0.378	1.14	0.395
14	0.978	0.400	1.10	0.449	1.13	0.440
16	0.938	0.450	1.11	0.504	1.13	0.418

Table 11: Lift (c_ℓ) and Drag (c_d) Sectional Coefficients for NACA 0012, S1 KFm, and S2 KFm at $\mathbf{Re} \approx 1.33 \times 10^5$. Rounded to 3 Significant Figures.

Angle of Attack (α in deg)	NACA 0012		S1 KFm		S2 KFm	
	c_ℓ	c_d	c_ℓ	c_d	c_ℓ	c_d
0	-0.0316	0.015	-0.0335	0.0349	-0.0462	0.0364
4	0.383	0.052	0.414	0.113	0.403	0.0934
10	0.889	0.192	1.15	0.230	1.09	0.263
12	1.04	0.318	1.13	0.380	1.12	0.354
14	0.998	0.398	1.12	0.456	1.09	0.341
16	0.96	0.454	1.11	0.504	1.12	0.341

Table 12: Lift (c_ℓ) and Drag (c_d) Sectional Coefficients for NACA 0012, S1 KFm, and S2 KFm at $\mathbf{Re} \approx 1.58 \times 10^5$. Rounded to 3 Significant Figures.

Angle of Attack (α in deg)	NACA 0012		S1 KFm		S2 KFm	
	c_ℓ	c_d	c_ℓ	c_d	c_ℓ	c_d
0	-0.0316	0.0132	-0.0318	0.0345	0.0439	0.0265
4	0.383	0.0435	0.416	0.107	0.402	0.0769
10	0.889	0.197	1.16	0.229	1.10	0.267
12	1.04	0.316	1.16	0.381	1.08	0.361
14	0.998	0.405	1.22	0.458	1.10	0.361
16	0.960	0.454	1.12	0.500	1.12	0.420

Table 13: Lift (c_ℓ) and Drag (c_d) Sectional Coefficients for NACA 0012, S1 KFm, and S2 KFm at $\mathbf{Re} \approx 1.81 \times 10^5$. Rounded to 3 Significant Figures.

Angle of Attack (α in deg)	NACA 0012		S1 KFm		S2 KFm	
	c_ℓ	c_d	c_ℓ	c_d	c_ℓ	c_d
0	-0.0248	0.0129	-0.0332	0.0342	-0.0440	0.0189
4	0.386	0.0474	0.414	0.0937	0.407	0.0633
10	0.965	0.231	1.17	0.228	1.09	0.276
12	1.13	0.309	1.18	0.378	1.10	0.361
14	1.03	0.403	1.22	0.486	1.10	0.405
16	0.980	0.454	1.15	0.499	1.09	0.429

continued on the next page

Table 14: Lift (c_ℓ) and Drag (c_d) Sectional Coefficients for NACA 0012, S1 KFm, and S2 KFm at $\mathbf{Re} \approx 2.00 \times 10^5$. Rounded to 3 Significant Figures.

Angle of Attack (α in deg)	NACA 0012		S1 KFm		S2 KFm	
	c_ℓ	c_d	c_ℓ	c_d	c_ℓ	c_d
0	-0.0244	0.0124	-0.0333	0.0341	-0.0428	0.0114
4	0.389	0.0525	0.416	0.0889	0.401	0.0612
10	0.973	0.232	1.17	0.227	1.14	0.246
12	1.14	0.234	1.17	0.374	1.08	0.350
14	1.06	0.397	1.23	0.488	1.08	0.350
16	0.977	0.413	1.14	0.496	1.14	0.408

continued on the next page

6.2 Theoretical Sectional Coefficient for a symmetrical thin airfoil

Angle of Attack (α in deg)	Theoretical c_ℓ
-12	-1.32
-8	-0.880
-4	-0.440
0	0.000
4	0.440
8	0.880
10	1.10
12	1.32

Table 15: Theoretical Sectional Lift Coefficient (c_ℓ) for a Thin Airfoil using $c_\ell = m_0\alpha$ ($m_0 = 0.11$ per degree). Rounded to 3 Significant Figures.